Cholesterol deprivation drives DHEA biosynthesis in human adrenals

Emanuele Pignatti[1,2], Emre Murat Altinkilic[1,2], Konstantin Bräutigam[3], Michael Grössl[2,4], Aurel Perren[3], Mihaela Zavolan[5], Christa E. Flück[1,2]

[1] Division of Pediatric Endocrinology, Diabetology and Metabolism, Department of Pediatrics, University Hospital Inselspital, University of Bern, 3010 Bern, Switzerland.

[2] Department for BioMedical Research, University Hospital Inselspital, University of Bern, 3010 Bern, Switzerland.

[3] Institute of Pathology, University of Bern, 3008 Bern, Switzerland.

[4] Department of Nephrology and Hypertension, Inselspital, Bern University Hospital, Freiburgstrasse 15, 3010, Bern, Switzerland.

[5] Biozentrum, University of Basel, 4056 Basel, Switzerland.

Short title: 'Cholesterol deprivation drives DHEA biosynthesis'

Keywords: adrenarche, DHEA, cholesterol

Corresponding Author: Emanuele Pignatti, Ph.D., Pädiatrische Endokrinologie/Diabetologie/Metabolik, Medizinische Universitätskinderklink Bern, Freiburgstrasse 15 / C843, 3010 Bern, Switzerland. ORCID: 0000-0002-5372-5692.

Name and E-mail address for reprint requests: Emanuele Pignatti, emanuele.pignatti@dbmr.unibe.ch

This work was funded by Uniscientia (C.E.F), the Novartis Foundation for Medical-Biological Research (C.E.F., 208015) and the NCCR RNA&Disease Translational Fellowship Grant (E.P.).

The authors have declared that no conflict of interest exists.

Abstract

Adrenarche is an early event in sexual maturation in prepubertal children and corresponds to the postnatal development of the adrenocortical zona Reticularis (zR). Still, the molecular mechanisms that govern the onset and maturation of zR remain unknown. Using tissue laser microdissection combined with transcript quantification and immunodetection, we showed that the human zR receives low levels of cholesterol in comparison to other adrenal layers. To model this metabolic condition, we challenged adrenal cells *in vitro* using cholesterol deprivation. This resulted in reprogramming the steroidogenic pathway towards inactivation of 3-beta-hydroxysteroid dehydrogenase type 2 (*HSD3B2*), increased *CYB5A* expression, and increased biosynthesis of Dehydroepiandrosterone (DHEA), three key features of zR maturation during adrenarche. Finally, we found that cholesterol deprivation leads to decreased transcriptional activity of POU3F2, which normally stimulates the expression of *HSD3B2* by directly binding to its promoter. These findings demonstrate that cholesterol deprivation can account, at least in part, for the acquisition of a zR-like androgenic program in humans.

Introduction

The adrenal cortex is an essential steroidogenic organ subdivided into three concentric morphologically and functionally different 'zones': the outer *zona Glomerulosa* (zG), the intermediate *zona Fasciculata* (zF), and the internal-most *zona Reticularis* (zR), which is responsible for the biosynthesis of adrenal androgens (1). While zG and zF are present in the adrenal cortex since birth, a morphologically distinguishable zR appears only around the age of 3 and progressively matures up to its adult size and function during adrenarche, in 6- to 8-year-old children (2). Harbingers of adrenarche in prepubertal children are increasing circulating levels of adrenal androgens, such as dehydroepiandrosterone (DHEA), its sulfated form (DHEA-S) and 11β-hydroxyandrostenedione, which eventually lead to clinical signs including growth of pubic and axillary hair, development of apocrine glands responsible for the adult-type body odor, and acne (2). Steroidogenesis in the zR is mediated by the zone-specific expression of critical enzymes and cofactors that convert the common precursor cholesterol into adrenal androgens, including cytochrome b5 (CYB5), and the low expression of 3β-hydroxysteroid dehydrogenase type 2 (HSD3B2). In fact, HSD3B2 is responsible for shunting the steroid pathway away from DHEA, while promoting the production of mineralocorticoids and glucocorticoids (1,2).

The molecular mechanisms that govern the formation of the zR remain ill-defined. The absence of adrenarche in dexamethasone-treated individuals and in patients carrying inactivating mutations in the receptor for the adrenocorticotropin hormone (ACTH) suggest that ACTH and its downstream Protein Kinase A (PKA)-mediated signaling are essential for zR maturation (3,4). While ACTH levels do nor rise in parallel with DHEA during prepubertal development (5,6), constitutive activation of PKA was recently shown to stimulate the formation of a functional zR-like zone in mice, which normally lack the zR and do not experience adrenarche (7). Altogether, these results indicate that the activation of the ACTH/PKA axis creates permissive conditions for the onset of the zR, but the underlying mechanisms are still elusive. Notably, PKA-stabilized

mouse adrenals show a marked activation of the *de novo* cholesterol biosynthesis pathway, pointing towards the possibility that cholesterol metabolism is implicated in zR formation.

To explore this hypothesis, we investigated enzymes associated with cholesterol metabolism in the human zR. We found that the zR receives low cholesterol supplies, which triggers the expression of genes implicated in *de novo* cholesterol synthesis (8). To model the impact of cholesterol shortage on adrenals, we challenged NCI-H295R adrenal cells using cholesterol deprivation. This led to increased DHEA synthesis, downregulation of *HSD3B2* expression, and increased expression of *CYB5A*, three key features of the human zR. We also found that cholesterol deprivation leads to decreased transcriptional activity of POU3F2, which normally stimulates the expression of *HSD3B2* by directly binding its promoter. Altogether, our data show that the molecular cascade initiated by cholesterol shortage explains, at least in part, the acquisition of a zR-like androgenic program.

Materials and Methods

Laser capture microdissection. Eight human adrenals were retrieved from fixed and paraffin-embedded blocks derived from patients with adrenal related or unrelated issues. Histologically normal regions of the adrenals were selected for dissection with the help of specialized pathologists. Laser capture microdissection was performed on 5µm sections on Polyethylene Naphthalate (PEN) membrane slides. Sections were deparaffinized and stained with hematoxylin following the manufacturer's instruction (Zeiss). Approximately $3x10^3 µm^3$ of adrenal material was captured onto an adhesive cap using a PALM Microbeam (Zeiss). A Quick-RNA™ FFPE Kit (Zymo Research) was used for RNA isolation according to the manufacturer's instructions. Reverse transcription and Real Time quantitative PCR (RT-qPCR) were conducted as described in the 'gene expression analysis' section.

Cell culture conditions. Human adrenocortical NCI-H295R cells were purchased from American Type Culture Collection (ATCC, CRL-2128). Cells at a passage between 13 and 20 were cultured as a monolayer at 37°C and 5% CO_2 in normal growth media (NGM) composed of DMEM/Ham's F-12 medium containing L-glutamine and 15mM HEPES medium (Thermo Fisher Scientific, 113300) supplemented with 5% NU-I serum (BD biosciences, 355500), 0.1% insulin, transferrin, and selenium (ITS; 100 U/ml; Thermo Fisher Scientific, 41400045), penicillin (100 U/ml) and streptomycin (100 µg/ml; Thermo Fisher Scientific, 15140122). 'Serum starvation' media (SS) was prepared as the NGM media without the addition of serum and ITS. Methyl-β-Cyclodextrin (MBCD; Sigma-Aldrich, C4555) was diluted in sterile deionized water to generate a 90mM stock and applied to NCI-H295R cells for 15 min at a concentration of 10mM in NGM. Dilutions were achieved using NCI-H295R cell culture media. Atorvastatin (MedChem Express, HY-B0589) was diluted in dimethyl sulfoxide (DMSO) to a concentration of 10mM. NCI-H295R cells were treated for 48h with 15µM atorvastatin diluted in NGM. To generate the POU3F2 transfection plasmid, the open reading frame of the gene (NM_005604.4) was cloned into a pcDNA3.1+/C-(K)-DYK

backbone (GenScript). Transfection in NCI-H295R cells was carried out using Lipofectamine 2000 (Thermo Fisher Scientific, 11668019) according to the manufacturer's instructions. Addition of human-derived high-density lipoproteins (HDL; Biorbyt, ORB81154) to cell media as cholesterol donors was carried out one day after plating, when 10µg/ml of cholesterol were added, and on the second day, when additional 40µg/ml of cholesterol were added. Knock-down experiments for *POU3F2* were performed using a TriFECTA® Kit (Integrated DNA Technologies - IDT), whereby three independent DsiRNA were tested for silencing efficacy based on RT-qPCR readout. The most efficient DsiRNA species was a double-strand oligonucleotide formed by the sequences CGUCUAACCACUACAGCCUGCUCAC and UCGCAGAUUGGUGAUGUCGGACGAGUG, and was used for the experiments within this work following the manufacturer's instructions. Briefly, 10nM DsiRNA and 1µl Lipofectamine™ RNAiMAX Transfection Reagent (Thermo Fisher Scientific, 13778075) were used on each well of NCI-H295R cells cultured in 6-well plates (3x10^5 cells per well). To maximize transfection efficiency, addition of DsiRNA and transfection reagent was contextual with cell plating. Media was changed at 48h from beginning of transfection. At 72h from beginning of transfection, cells were collected in TRI Reagent (Sigma, T9424) and processed for gene expression analysis (see dedicated paragraphs below).

*Immunofluorescence and microscopy***.** We performed protein immunodetection on the same adrenal samples used for laser capture microdissection (see dedicated paragraph above). Five mm-thick sections were cut on Fisherbrand™ Superfrost™ Plus Microscope Slides (Fisher Scientific, 12-550-15) and processed for immunostaining by stepwise rehydration and permeabilization with 50mM Tween-20 in PBS. Antigen retrieval was performed in 10mM Sodium Citrate pH 6.0. Blocking and indirect staining were carried out using the following kits from Thermo Fisher Scientific, following the manufacturer's instructions: Alexa Fluor™ 488 Tyramide SuperBoost™ Kit, goat anti-rabbit IgG (B40943), and Alexa Fluor™ 647 Tyramide SuperBoost™

Kit, goat anti-mouse IgG (B40916). Direct staining was performed using the following primary antibodies: anti-AKR1C3 (mouse monoclonal, Sigma, A6229; RRID: AB_476751); anti-CYB5A (mouse monoclonal, Abnova, H00001528-M05; RRID: AB_2089958); anti-FDPS (rabbit polyclonal, Novusbio, NBP1-89509; RRID: AB_11020229); anti-MVD (rabbit polyclonal, Novusbio, NBP2-13628; RRID: AB_2910645); anti-ApoB (rabbit polyclonal, Novusbio, NBP2-38608; RRID: AB_2910644). All primary antibodies were used at a 1:200 dilution. Sections were counter-stained with DAPI (40 ,6-diamidino-2-phenylindole) and mounted in Prolong Gold Mount Solution (Thermo Fisher Scientific, P36934). Images were captured with a Nikon Eclipse Ti-E upright microscope.

*Gene expression analysis***.** RNA was purified from cell monolayers using TRI Reagent (Sigma, T9424) and Direct-zol RNA kits (Zymo Research, R2051), following the manufacturer's instructions. RNA was reverse transcribed into cDNA using the High-Capacity cDNA Reverse Transcription Kit (Thermo Fisher Scientific, 4368814). Gene expression analysis was performed by RT-qPCR using the QuantStudio 1 thermocycler (Life Technologies) and the PowerUp™ SYBR™ Green Master Mix (Thermo Fisher Scientific, A25780), according to manufacturer's instructions. Technical duplicates were used to control for technical variability. *GAPDH* or *PPIA* transcripts were used as the internal controls and data were expressed using the 2^{-ddCt} method. Sample size was estimated based on the published literature and our experience and is indicated in the figure legends. The primers used for RT-qPCR were as follows: *HSD3B2*: Fw, CCACACCGCCTGTATCATTG Rv, ACACAGGCCTCCAACAGTAG. *CYB5A*: Fw, AAGGTGTACGATTTGACCAA Rv, CGACATCCTCAAAGTTCTCA. *HMGCR*: Fw, CGATGCTCTTGTTGAATGTC Rv, GCAGCACATAATTTCAAGCT. *SQLE*: Fw, TCATCAGTGAAGAAACGAGG Rv, TCATTCCTCCACCAGTAAGT. *HMGCS1*: Fw, CTGCTATTCTGTCTACTGCA Rv, TGAAAGATCATGAAGCCAAA. *LSS*: Fw, ATGACATTTTACGTGGGGC Rv, CGCACAATCTCTTCTCTGTA. *ABCG1*: Fw,

GATGAAGGCAGAAGGGAAAT Rv, CATGACTGGAGGGTTGTTC. *LDLR*: Fw, GGTGGAGATAGTGACAATGT Rv,. CTACTGGGCTTCTTCTCATT *FDPS*: Fw, CAGAACAGTACCAGATCCTG Rv, TCCTCATATAGCGCCTTCA. *MVD*: Fw, CCAATGCCGTGATCTTCA Rv, TTCAGAAACGTGTCTCCATT. *GAPDH*: Fw, GCTCTCTGCTCCTCCTGTTC Rv, CGACCAAATCCGTTGACTCC. *PPIA*: Fw, CCAGGGTTTATGTGTCAGGG Rv, AAGATGCCAGGACCCGTATG.

Steroid profiling. Steroids were quantified by high resolution liquid chromatography- tandem mass spectrometry (LC-MS/MS). Quantification was performed using an in-house developed method based on the approach by Peitzsch et al. (9). Briefly, 500µL of media were spiked with isotopically labelled standards, followed by addition of 250µL of zinc sulphate (0.1 mol/L) and 500µL of cold methanol (-20°C) for protein precipitation and steroid extraction. Samples were vortexed and centrifuged for 5 min at 8000g. 250µL of water was added to each sample and purified by solid phase extraction on an OasisPrime HLB 96-Well Plate (Waters, 186008054) using a positive pressure 96-well processor (Waters, 186006961). LC-MS measurements were performed using Vanquish UHPLC coupled to a QExactive Orbitrap Plus (both from Thermo Fisher Scientific). All data were processed using TraceFinder 4.0 (Thermo Fisher Scientific). For each sample, concentration data were normalized by the total amount of steroids, and the average of normalized values for controls was set to 100, unless indicated otherwise.

Transcriptome profiling. RNA was purified from cell monolayers using TRI Reagent (Sigma, T9424) and Direct-zol RNA kits (Zymo Research, R2051), following the manufacturer's protocol. RNA integrity was assessed on a TapeStation instrument (Agilent Technologies) using RNA ScreenTape (Agilent, 5067-5576). Quantification was carried out using a QuantiFluor RNA System (Promega, E3310). Library preparation was performed from 200ng total RNA using the TruSeq Stranded mRNA Library Kit (Illumina, 20020594) and the TruSeq RNA UD Indexes

(Illumina, 20020590). 15 cycles of PCR were performed. Libraries were quality-checked on a Fragment Analyzer (Advanced Analytical) using the Standard Sensitivity NGS Fragment Analysis Kit (Advanced Analytical, DNF-474) revealing excellent quality of libraries (average concentration: 145±43 nmol/L, average library size: 339±8 base pairs). Samples were pooled to equal molarity. The pool was quantified by Fluorometry using the QuantiFluor ONE dsDNA System (Promega, E4871). Libraries were sequenced Single-reads 76 bases using a NextSeq 500 High Output Kit 75-cycles (Illumina, 20024906) loaded at 1.8pM and including 1% PhiX. Primary data analysis was performed with a Illumina RTA version 2.4.11. On average per sample: 38.9±5.4 million Passed-filtered (PF) reads were collected on 1 NextSeq 500 Flow-Cell. Kallisto v0.46.2 was used for alignment and quantification. The expression of each transcript t_i was then estimated in units of transcripts per million (TPM) by dividing the read count c_i corresponding to the transcript by the transcript length l_i and normalizing to the library size:

$$t_i = \frac{\frac{c_i}{l_i}}{\sum_{j=1}^{\#\ of\ transcripts} \frac{c_j}{l_j}} \cdot 10^6.$$

The expression level of a gene was calculated as the sum of normalized expression levels of transcripts associated with the gene. For every gene, read counts of were also summed up and further used for the differential expression analysis. Differential expression analysis was performed with EdgeR available through the R/Bioconductor package (10). As the input we used a processed data set with four biological replicates per condition. A gene was included in the analysis only if it had at least 30 counts per million (CPM) as average across the control samples. Gene expression was considered statistically different between two conditions if the false discovery rate (FDR) was less than 0.1 (11). Transcriptome profiling analysis was performed using the GSEA 4.0.2 software (Broad Institute, MA, USA; San Diego University, CA, USA), and applying all the ontology gene sets. Volcano plot was generated using the ShinyVolcanoPlot online tool (https://paolo.shinyapps.io/ShinyVolcanoPlot/). The heat map was created using the

Morpheus online tool (Broad Institute, MA, USA). The generated datasets are available on the GEO repository (accession number: GSE191180).

Chromatin immunoprecipitation (ChIP) assay.

For ChIP assay, NCI-H295R cells were cultured up to about 70% confluency on 175cm^2 flasks. Fixation, quenching, lysis, and chromatin shearing were performed using the truChIP® Chromatin Shearing Kit (Covaris, 520237), following the manufacturer's instructions. Chromatin was sheared for 5 min using milliTUBE 1ml AFA Fiber tubes (Covaris, 520135) on a E220evolution Focused-ultrasonicator (Covaris). Efficient shearing (fragments between 200 and 700bp) was assessed by running about 1µg of chromatin on a 1% agarose gel. Protein G-agarose/salmon sperm DNA beads (Sigma, 16-201) were used for preclearing and antibody precipitation. The following antibodies were used for incubation with the sheared chromatin overnight at 4°C: anti-POU3F2/OCT7, rabbit polyclonal (Novusbio, NBP2-21585; RRID: AB_2910643); Rabbit IgG Isotype Control (Bioss, bs-0295P; RRID: AB_2832980) as control for nonspecific binding. De-crosslinking was achieved by incubating immunoprecipitated chromatin with 250mM NaCl overnight at 65°C and 400µg/ml Proteinase K (Zymo Research, D3001-2-5) at 60°C for 1 h. DNA was isolated using the NucleoSpin Gel and PCR Clean-up (Macherey-Nagel, 740609.50). Chromatin enrichment was quantified using RT-qPCR (see Gene Expression Analysis section) and the following primers: *HSD3B2*_BS: Fw, GGCTAAAATAGATCTCCCTCC Rv, GGATCTGCAATCTGTGAACT. *VRK*_BS: Fw, CCAGCTGAGGACTTTTAGAA Rv, CCTTCCAGCCATAAGTTACA. Binding of POU3F2 to a consensus sequence within the minimal promoter of *VRK2* was used as positive control for the experiment (12).

Transcriptional activity assay. NCI-H295R cells were transfected with empty pGL3 firefly reporter vector or pGL3 vectors carrying the *HSD3B2* promoter elements (1050 base pairs upstream the transcriptional start site of the *HSD3B2* gene). The empty pcDNA3.1+/C-(K)-DYK backbone

(GenScript) or the *POU3F2* expression plasmid, generated as described in the 'Cell culture conditions' paragraph, were also used. Transfection was carried out on NCI-H295R cell monolayers in 12-well plates, using a total of 2.5µg DNA plasmid and the Lipofectamine 2000 reagent (Thermo Fisher Scientific, 11668019), according to the manufacturer's instructions. 100ng of Renilla luciferase reporter (pRL-TK) was also added to every well to control for baseline response. Firefly and Renilla reporters were revealed using the Dual-Luciferase Reporter Assay System (Promega, 16185). Bioluminescence was measured using a SpectraMax M2 microplate reader (Molecular Devices).

Statistics. Two-tailed Student's t-test was used for comparisons between any two groups, unless specified otherwise. For every comparison, the F-test was used to evaluate whether the two groups had different variances. If this was the case, the two-tailed Welch t test was used. One-Way ANOVA and Tukey post hoc analysis were used for comparisons among four groups, unless specified otherwise. Prism 9 software (GraphPad) was used for statistical analysis. Outliers were flagged and excluded using the method of Tukey's fences. The statistical details of the experiments can be found in the figure legends, whereby 'n' values correspond to the number of independent samples. Data are presented as Mean ± Standard Error of the Mean (SEM).

Study approval. Human material was collected and used in agreement with the Swiss Ethics Committee authorization (BASEC ID 2019-01582).

Results

The human zona Reticularis (zR) receives low cholesterol supplies.

Cellular cholesterol is supplied either by uptake from the extracellular environment or *de novo* synthesis and is cleared by specialized ATP-binding cassette (ABC) transporters responsible for cholesterol export.

To begin to understand the features of cholesterol metabolism in the adrenal zR, we isolated the zR and the neighboring *zona Fasciculata* (zF, used as reference) from human adrenal glands using laser capture microdissection (Fig. 1A). RNA was purified from the dissected material, and quantification of transcripts encoding HSD3B2 (enriched in the zF) and CYB5A (enriched in the zR) was used to validate the specificity of tissue acquisition (Fig. 1B). To assess the activation of *de novo* cholesterol synthesis in the zR, we quantified the expression of the two rate-limiting enzymes involved in cholesterol production, *HMGCR* (HMG-CoA reductase) and *SQLE* (Squalene monooxygenase), and two enzymes involved in the biosynthesis of critical intermediates, *HMGCS1* (Hydroxymethylglutaryl-CoA synthase) and *LSS* (Lanosterol synthase). All these transcripts resulted enriched in the zR, suggesting that this region is engaged in cholesterol production more than the neighboring zF (Fig. 1C). To confirm the zR-specific increase of enzymes involved in *de novo* cholesterol synthesis, we carried out the immunodetection of two additional enzymes, FDPS (Farnesyl pyrophosphate synthase) and MVD (Mevalonate diphosphate decarboxylase), in human adrenals. Both proteins resulted enriched in the AKR1C3-expressing zR (Fig. 1D).

To gain more insight into the status of cholesterol metabolism in the zR, we quantified the messenger RNAs of ABCG1 and LDLR, two membrane proteins responsible for excretion and uptake of cholesterol, respectively. Quantification showed that the zR expresses low levels of *ABCG1* and an increased trend of *LDLR* expression in comparison with the neighboring zF (Fig. 1E), indicating that the zR displays a molecular profile consistent with cholesterol shortage (8).

Finally, to determine whether the zR is exposed to low cholesterol supplies, we performed immunostaining for apolipoprotein B (ApoB), which is the primary apolipoprotein for a series of cholesterol-donor particles including low-density lipoproteins (LDLs). This experiment revealed that ApoB is distributed in a gradient fashion throughout the human adrenal, whereby the outer cortical regions are richer in ApoB with respect to the innermost CYB5A-positive zR, which displays weak immunoreactivity. Altogether, our data indicate that the human zR is exposed to lower levels of cholesterol with respect to the neighboring zones, and this triggers the local activation of the cholesterol biosynthesis pathway.

Cholesterol deprivation in adrenocortical cells replicates key features of the human zR.

To further study the implications of cholesterol shortage and increased *de novo* cholesterol synthesis in an adrenal model, we reproduced these metabolic conditions in the NCI-H295R adrenal cell line. Specifically, we deprived NCI-H295R cells of cholesterol by either culturing them in a serum-free medium or depriving plasma membranes of cholesterol using lipid-free methyl-β-cyclodextrins (MBCD). To quantify the extent of cholesterol synthesis activation, we assessed the transcripts encoding key enzymes including FDPS, HMGCR, HMGCS1, MVD, LSS and SQLE. As expected, both experimental models resulted in the activation of cholesterol synthesis by increasing the expression of some or all the genes taken into consideration within 24h-48h of cholesterol deprivation (Fig. 2A). To be able to survey the full impact of cholesterol deprivation, we performed all further experiments at 48h.

To assess the effect of cholesterol deprivation on steroidogenic activity, we quantified media contents of DHEA, which reflects zR output in human adrenals (Fig. 2B). Instead, cortisol levels were measured as a proxy for zF activity. Notably, both serum starvation and treatment with MBCD led to an increased production of DHEA and a decreased synthesis of cortisol (Fig. 2C), which indicates that cholesterol deprivation reprograms steroidogenesis toward a zR-like profile.

To understand what molecular mechanisms lead to increased DHEA following cholesterol deprivation, we quantified the transcripts encoding HSD3B2, whose reduction is a hallmark of human zR (Fig. 2B). Importantly, *HSD3B2* transcripts resulted lower following both treatments (Fig. 2D), indicating that the regulation of this enzyme can account at least in part for the zR-like steroid output following cholesterol deprivation. To confirm that the effect of serum starvation on DHEA production and *HSD3B2* transcripts is a cholesterol-dependent mechanism, we exposed serum starved cells to cholesterol-loaded HDL particles. As expected, addition of HDL reverted the starvation phenotype by decreasing DHEA production and increasing *HSD3B2* expression (Fig. 2E). Finally, we quantified the transcripts encoding CYB5A, a critical cofactor for CYP17A1 lyase activity during zR maturation and observed an increase in transcription following MBCD exposure (Fig. 2F).

The pathway leading to *de novo* cholesterol synthesis is also known to contribute precursors for protein prenylation and ubiquinone, which have important effects on several aspects of cell metabolism (13). Therefore, to rule out that the reprogramming of the steroidogenic pathway toward DHEA production is a consequence of *de novo* cholesterol synthesis pathway byproducts, we exposed untreated and cholesterol deprived cells to atorvastatin, a potent inhibitor of HMGCR, which mediates one of the earliest enzymatic conversions in the process of cholesterol biosynthesis. As expected, atorvastatin did not generate a difference in *HSD3B2* transcripts in either cholesterol deprivation model (Fig. 2G). This result indicates that the metabolic reprogramming in response to cholesterol deprivation is uniquely due to cholesterol deprivation and is not mediated by the activation of *de novo* cholesterol synthesis or any of its byproducts.

Altogether, our findings indicate that cholesterol deprivation in adrenocortical cells replicate key features of the zR, including increased DHEA production, suppression of *HSD3B2* transcripts and increased transcription of *CYB5A*.

POU3F2 mediates the effects of cholesterol deprivation on HSD3B2.

To gain further insight into the molecular mechanisms that lead to increased DHEA production in NCI-H295R cells, we profiled the transcriptome of serum starved cells and compared it with cells grown in normal growth media. Using a cutoff fold change of 1.5 and 0.1 as false discovery rate, we found 93 up-regulated and 94 down-regulated transcripts in starved cells (Fig. 3A). As expected, *HSD3B2* was among the downregulated genes (Fig. 3B). Gene Set Enrichment analysis of the GO terms that were significantly up-regulated following serum starvation included '*Regulation of cholesterol biosynthetic process*', which further confirmed that a set of genes involved in the *de novo* cholesterol biosynthetic pathway are positively regulated by cholesterol deprivation (Fig. 3C, D). Specifically, *HMGCS1*, *MVD*, *LSS* and *FDPS* genes appeared among the upregulated transcripts, while *ABCG1* was down-regulated in cholesterol-deprived cells (Fig. 3E).

Then, we sought to predict the transcription factors that could account for the decreased *HSD3B2* expression in cholesterol deprived cells. For this purpose, we used ISMARA (Integrated System for Motif Activity Response Analysis) (14), an online tool (https://ismara.unibas.ch/mara/) that models data from RNA sequencing in terms of computationally predicted regulatory sites for transcription factors. To select the transcription factors with a differential predicted activity upon serum starvation compared to cells grown in normal growth media, we set a significant threshold (≥ 2) based on the ISMARA-reported standard score (z-value). Besides, we further shortlisted the factors for their potential binding to ISMARA-detected consensus binding sites on the promoter regions of *HSD3B2*. We found 5 groups of transcription factors whose activity was predicted to change upon serum starvation based on our RNA sequencing data (Fig. 4A). Among these factors, POU3F2 was the only one to show a significant potential for influencing *HSD3B2* expression (based on standard score), via binding one conserved putative site identified by ISMARA located between -94 and -80 base pairs upstream the *HSD3B2* transcriptional start site (TSS), corresponding to the GTGCAATGTAAATGT sequence (Fig. 4B). To determine whether POU3F2 effectively binds this site, we immunoprecipitated chromatin of NCI-H295R cells using

an antibody raised against POU3F2 and found an enrichment of the predicted sequence (Fig. 4C). In addition, luciferase assay using the promoter region of *HSD3B2* (-1050 upstream the TSS) revealed significant transcriptional activity following stimulation with POU3F2 (Fig. 4D).

To determine the impact of POU3F2 on *HSD3B2* expression, we inhibited POU3F2 translation, which resulted in the reduction of *HSD3B2* transcripts (Fig. 4E). Finally, we drove POU3F2 overexpression in serum starved NCI-H295R cells, which led to increased *HSD3B2* expression and decreased production of DHEA, consistent with a role for POU3F2 in the control of the steroidogenic program typical of the zR (Fig. 4F).

Discussion

The establishment of a functional zR within the adrenal cortex, referred to as adrenarche, is an early event in prepubertal sexual maturation, since it anticipates pubarche and activation of the central gonadotropic axis (15,16). While the enzymes and cofactors involved in the zR program have been deciphered, the mechanisms governing the onset of adrenarche remain unclear. Our data show that the human zR is exposed to poor cholesterol supplies in comparison with the neighboring zF zone, and this triggers the zR-specific activation of genes involved in *de novo* cholesterol biosynthesis (8). This in agreement with previous evidence based on incorporation of acetate-2-14C into newly synthetized cholesterol in human adrenals, whereby cholesterol biosynthesis was found to be several times higher in the zR with respect to the zF (17).

We demonstrate that cholesterol restriction in cells leads to reprogramming the steroidogenic activity towards features that are typical of the zR, including suppression of *HSD3B2* expression, increased *CYB5A* expression, and consequent upregulation of DHEA biosynthesis. While we previously showed that serum starvation of NCI-H295R cells resulted in increased androgenic output (18), we could never narrow down, until now, that cholesterol deprivation accounted for this effect. Still, we cannot rule out that additional factors can contribute to changes in HSD3B2 activity and increased biosynthesis of DHEA. For instance, Majzoub and Topor recently hypothesized that increasing concentrations of intradrenal cortisol in prepubertal children directly result in the competitive inhibition of HSD3B2 (19). Indeed, we argue that the onset of adrenarche may be a multifactorial event, whereby several molecular and environmental cues converge towards the maturation of a functional zR. In line with this hypothesis, several studies have shown a connection between premature adrenarche and disorders including functional ovarian hyperandrogenism or certain aspects of the metabolic syndrome (reviewed in (20,21)). This suggests that lipid and glucose metabolism could also be implicated in timing the onset of adrenarche, and further studies are needed to narrow down the critical contributors.

Our results also show a reprogramming role for cholesterol in the adrenal and provide therefore a paradigm for possible reprogramming roles of cholesterol also in other tissues. Such a role has already been established for cholesterol in pathological conditions: for instance, increased cholesterol biosynthesis has been associated with promotion of initiation and/or progression of several malignant forms, including breast and prostate cancers, and hepatocellular carcinoma, whereby cholesterol biproducts oxysterols and prenylation intermediaries favor the activation of downstream tumorigenic pathways (13). Indeed, the use of statins and other drugs that aim at reducing cholesterol biosynthesis or cellular availability has been approved, or is under clinical study, for several malignant forms (13). Cholesterol has also been recently implicated in the biology of the sonic hedgehog signaling pathway, with clear implications in tumor initiation, progression and metastasis, and in the fields of developmental and adult stem cell biology (22).

Finally, we show that POU3F2 binds the *HSD3B2* promoter and stimulates its expression. Suppression of *POU3F2* translation results in decreased *HSD3B2* transcripts, while expression of POU3F2 in cholesterol deprivation models rescues *HSD3B2* levels and lowers the production of DHEA. However, we did not observe a reduction of *POU3F2* transcripts upon cholesterol deprivation (data not shown), which suggests that POU3F2 may be regulated at a posttranscriptional level, as previously described in melanocytes (23). In line with this hypothesis, we observed a significant, but not dramatic, change in both *HSD3B2* and DHEA following POU3F2 overexpression of NCI-H295R cells, which may indicate that POU3F2 needs additional modifications for being fully active. We also cannot exclude the possibility that other molecular factors may produce a negative effect on POU3F2 transcriptional activity, and additional molecular pathways need to be engaged to release this negative action. Indeed, we previously demonstrated that the regulation of the *HSD3B2* promoter is mediated by an interplay of several transcriptional regulators (24), which indicates that POU3F2 must be part of a complex transcriptional machinery.

In conclusion, we demonstrate that cholesterol shortage is a feature of the human zR and promotes a zR-like steroidogenic reprogramming in cells. Our findings establish a new paradigm for the onset of adrenarche, whereby cholesterol levels could play a role in initiating the typical zR steroidogenic program.

Author contributions

E.P., C.E.F. and M.Z. designed the project. E.P. carried out all the experiments, unless otherwise stated. E.M.A. performed the luciferase assay. M.G. performed the LC-MS/MS experiments. K.B. and A.P. provided the human material. A.P. and M.Z. provided important intellectual contribution. C.E.F. supervised the whole work. E.P. wrote the manuscript and all authors provided editorial input.

Acknowledgements

This work was funded by Uniscientia (C.E.F), the Novartis Foundation for Medical-Biological Research (C.E.F., 208015) and the NCCR RNA&Disease Translational Fellowship Grant (E.P.). The authors wish to thank Alexander Kanitz, Anastasiya Boersch, Pamela Nicholson, Philippe Demougin, Silvia Rihs, Kay Sauter and Idoia Martínez de LaPiscina for suggestions and experimental help. Thanks also to Nicoletta Sorvillo for helpful discussion.

Data Availability

Some or all datasets generated during and/or analyzed during the current study are not publicly available but are available from the corresponding author on reasonable request.

References

1. **Pignatti E, Flück CE.** Adrenal cortex development and related disorders leading to adrenal insufficiency. *Mol Cell Endocrinol* 2021;527:111206.

2. **Witchel SF, Pinto B, Burghard AC, Oberfield SE.** Update on adrenarche. *Current Opinion in Pediatrics* 2020;32(4):574–581.

3. **Kim MH, Hosseinian AH, Dupon C.** Plasma levels of estrogens, androgens and progesterone during normal and dexamethasone-treated cycles. *J Clin Endocrinol Metab* 1974;39(4):706–712.

4. **Weber A, Clark AJ, Perry LA, Honour JW, Savage MO.** Diminished adrenal androgen secretion in familial glucocorticoid deficiency implicates a significant role for ACTH in the induction of adrenarche. *Clin Endocrinol (Oxf)* 1997;46(4):431–437.

5. **Mellon SH, Shively JE, Miller WL.** Human proopiomelanocortin-(79-96), a proposed androgen stimulatory hormone, does not affect steroidogenesis in cultured human fetal adrenal cells. *J Clin Endocrinol Metab* 1991;72(1):19–22.

6. **Penhoat A, Sanchez P, Jaillard C, Langlois D, Bégeot M, Saez JM.** Human proopiomelanocortin-(79-96), a proposed cortical androgen-stimulating hormone, does not affect steroidogenesis in cultured human adult adrenal cells. *J Clin Endocrinol Metab* 1991;72(1):23–26.

7. **Dumontet T, Sahut-Barnola I, Septier A, Montanier N, Plotton I, Roucher-Boulez F, Ducros V, Lefrançois-Martinez A-M, Pointud J-C, Zubair M, Morohashi K-I, Breault DT, Val P, Martinez A.** PKA signaling drives reticularis differentiation and sexually dimorphic adrenal cortex renewal. *JCI Insight* 2018;3(2). doi:10.1172/jci.insight.98394.

8. **Luo J, Yang H, Song B-L.** Mechanisms and regulation of cholesterol homeostasis. *Nat Rev Mol Cell Biol* 2020;21(4):225–245.

9. **Peitzsch M, Dekkers T, Haase M, Sweep FCGJ, Quack I, Antoch G, Siegert G, Lenders JWM, Deinum J, Willenberg HS, Eisenhofer G.** An LC-MS/MS method for steroid profiling during adrenal venous sampling for investigation of primary aldosteronism. *J Steroid Biochem Mol Biol* 2015;145:75–84.

10. **Robinson MD, McCarthy DJ, Smyth GK.** edgeR: a Bioconductor package for differential expression analysis of digital gene expression data. *Bioinformatics* 2010;26(1):139–140.

11. **Benjamini Y, Hochberg Y.** Controlling the False Discovery Rate: A Practical and Powerful Approach to Multiple Testing. *Journal of the Royal Statistical Society: Series B (Methodological)* 1995;57(1):289–300.

12. **Pearl JR, Colantuoni C, Bergey DE, Funk CC, Shannon P, Basu B, Casella AM, Oshone RT, Hood L, Price ND, Ament SA.** Genome-Scale Transcriptional Regulatory Network Models of Psychiatric and Neurodegenerative Disorders. *Cell Systems* 2019;8(2):122-135.e7.

13. **Huang B, Song B, Xu C.** Cholesterol metabolism in cancer: mechanisms and therapeutic opportunities. *Nat Metab* 2020;2(2):132–141.

14. **Balwierz PJ, Pachkov M, Arnold P, Gruber AJ, Zavolan M, van Nimwegen E.** ISMARA: automated modeling of genomic signals as a democracy of regulatory motifs. *Genome Res* 2014;24(5):869–884.

15. **Auchus RJ.** The Physiology and Biochemistry of Adrenarche. In: Ghizzoni L, Cappa M, Chrousos GP, Loche S, Maghnie M, eds. *Endocrine Development*.Vol 20. S. Karger AG; 2011:20–27.

16. **Witchel SF.** Congenital Adrenal Hyperplasia. *J Pediatr Adolesc Gynecol* 2017;30(5):520–534.

17. **Borkowski A, Delcroix C, Levin S.** Metabolism of adrenal cholesterol in man. II. In vitro studies including a comparison of adrenal cholesterol synthesis with the synthesis of the clucocorticosteroid hormones. *J Clin Invest* 1972;51(7):1679–1687.

18. **Kempná P, Hirsch A, Hofer G, Mullis PE, Flück CE.** Impact of Differential P450c17 Phosphorylation by cAMP Stimulation and by Starvation Conditions on Enzyme Activities and Androgen Production in NCI-H295R Cells. *Endocrinology* 2010;151(8):3686–3696.

19. **Majzoub JA, Topor LS.** A New Model for Adrenarche: Inhibition of 3β-Hydroxysteroid Dehydrogenase Type 2 by Intra-Adrenal Cortisol. *Horm Res Paediatr* 2018;89(5):311–319.

20. **Utriainen P, Laakso S, Liimatta J, Jääskeläinen J, Voutilainen R.** Premature Adrenarche - A Common Condition with Variable Presentation. *Horm Res Paediatr* 2015;83(4):221–231.

21. **Rosenfield RL.** Normal and Premature Adrenarche. *Endocrine Reviews* 2021:bnab009.

22. **Radhakrishnan A, Rohatgi R, Siebold C.** Cholesterol access in cellular membranes controls Hedgehog signaling. *Nat Chem Biol* 2020;16(12):1303–1313.

23. **Berlin I, Denat L, Steunou A-L, Puig I, Champeval D, Colombo S, Roberts K, Bonvin E, Bourgeois Y, Davidson I, Delmas V, Nieto L, Goding CR, Larue L.** Phosphorylation of BRN2 modulates its interaction with the Pax3 promoter to control melanocyte migration and proliferation. *Mol Cell Biol* 2012;32(7):1237–1247.

24. **Udhane S, Kempna P, Hofer G, Mullis PE, Flück CE.** Differential regulation of human 3β-hydroxysteroid dehydrogenase type 2 for steroid hormone biosynthesis by starvation and cyclic AMP stimulation: studies in the human adrenal NCI-H295R cell model. *PLoS ONE* 2013;8(7):e68691.

Figure Legends

Figure 1. The human zona Reticularis (zR) is exposed to low cholesterol supplies. A) Schematic representation of the regions of the adrenal cortex that have been dissected using laser capture microdissection. B, C and E) Quantification of transcripts within the zR with respect to the zona Fasciculata. Statistical analysis was performed using a paired t-test. n= 8 independent adrenals. D and F) Co-immunostaining of human adrenal sections. The dotted lines delimit the borders of the zR and are drawn based on zR-specific AKR1C3 or CYB5A staining. n=3 independent adrenals each staining. Scale bar, 100µm. c, capsule; zG, zona Glomerulosa; zF, zona Fasciculata; zR, zona Reticularis; med, medulla. *, $p \leq 0.05$; **, $p \leq 0.01$; ***, $p \leq 0.001$; ****, $p \leq 0.0001$.

Figure 2. Cholesterol deprivation leads to decreased *HSD3B2,* and increased CYB5A and DHEA production. A) Quantification of transcripts involved in *de novo* cholesterol synthesis following cholesterol deprivation by serum starvation (SS, left graph) or Methyl-β-cyclodextrins (MBCD, right). The orange dotted lines indicate the baseline expression. B) Schematic representation of the pathways leading to DHEA and cortisol production in the zR and zF, respectively, from the common precursor cholesterol, and the gatekeeping role of the 3-beta-hydroxysteroid dehydrogenase type 2 (HSD3B2) enzyme. C) DHEA and cortisol quantification in NCI-H295R cells media following SS or MBCD treatment with respect to control cells cultured in normal growth media (NGM). D and G) Quantification of *HSD3B2* transcripts following exposure to SS or MBCD treatment, and in combination with Atorvastatin (G). E) Quantification of DHEA in media and *HSD3B2* transcripts in cells cultured in SS media with or without the supplementation of high-density lipoproteins (HDL). Due to the important impact of HDL on overall steroidogenesis, data are normalized to total steroid amount and to the amount of pregnenolone in each sample. F) Quantification of transcripts encoding CYB5A following MBCD treatment. All experiment were

run using both biological and technical triplicates. ns, not significant; *, $p \leq 0.05$; **, $p \leq 0.01$; ***, $p \leq 0.001$; ****, $p \leq 0.0001$.

Figure 3. The transcriptome of cholesterol deprived cells mimics the molecular profile of the human zR. A) Volcano plot depicting the distribution of transcripts based on the extent of differential expression (x axis) and significance (y axis) following serum starvation of NCI-H295R cells. B) Normalized expression values of the *HSD3B2* transcripts following serum starvation of NCI-H295R cells. Statistical analysis was carried out using a paired t-test. C) Gene Ontology (GO) terms enriched in serum starved NCI-H295R cells based on Gene Set Enrichment Analysis (GSEA), with focus on the 'Regulation of cholesterol biosynthetic process' term (D). E) Heat map reporting the differentially expressed transcripts within the 'Regulation of cholesterol biosynthetic process' GO term. NGM, normal growth media. SS, serum starvation. logFC, logarithmic fold change. FDR, False Discovery Rate.

Figure 4. POU3F2 mediates the effects of cholesterol deprivation on *HSD3B2*. A) Transcription factors predicted to change their transcriptional activity on *HSD3B2* following serum starvation of NCI-H295R cells using Integrated System for Motif Activity Response Analysis (ISMARA) (14). B) Schematic representation of the potential POU3F2 *cis*-binding site within the promoter of the *HSD3B2* gene (94-80 base pairs upstream the transcriptional start site). C) Binding of POU3F2 to the candidate sequence on the *HSD3B2* promoter was tested using chromatin immunoprecipitation assay. Binding to an established consensus sequence in the *VRK2* gene was used as positive control. Paired results from IgG control and POU3F2 antibodies were both normalized to the corresponding IgG values. Statistical analysis was performed using a paired t-test. D) Luciferase assay was used to test the transcriptional activity of POU3F2 on the *HSD3B2* promoter region (-1050 with respect to the transcriptional start site). E) Quantification of

transcripts encoding POU3F2 and HSD3B2 following transfection of a negative control Dicer-substrate small interfering (Dsi)RNA or a DsiRNA targeting *POU3F2*. F) Expression of *HSD3B2* and production of DHEA in cells transfected with either a POU3F2 expressing plasmid or an empty vector as control. All experiment were run as biological and technical triplicates, apart from experiments in panel E), where technical duplicates were used. In C), only technical averages are displayed. EV, empty vector. Prom., promoter. *, $p \leq 0.05$; ****, $p \leq 0.0001$.

Figure 1

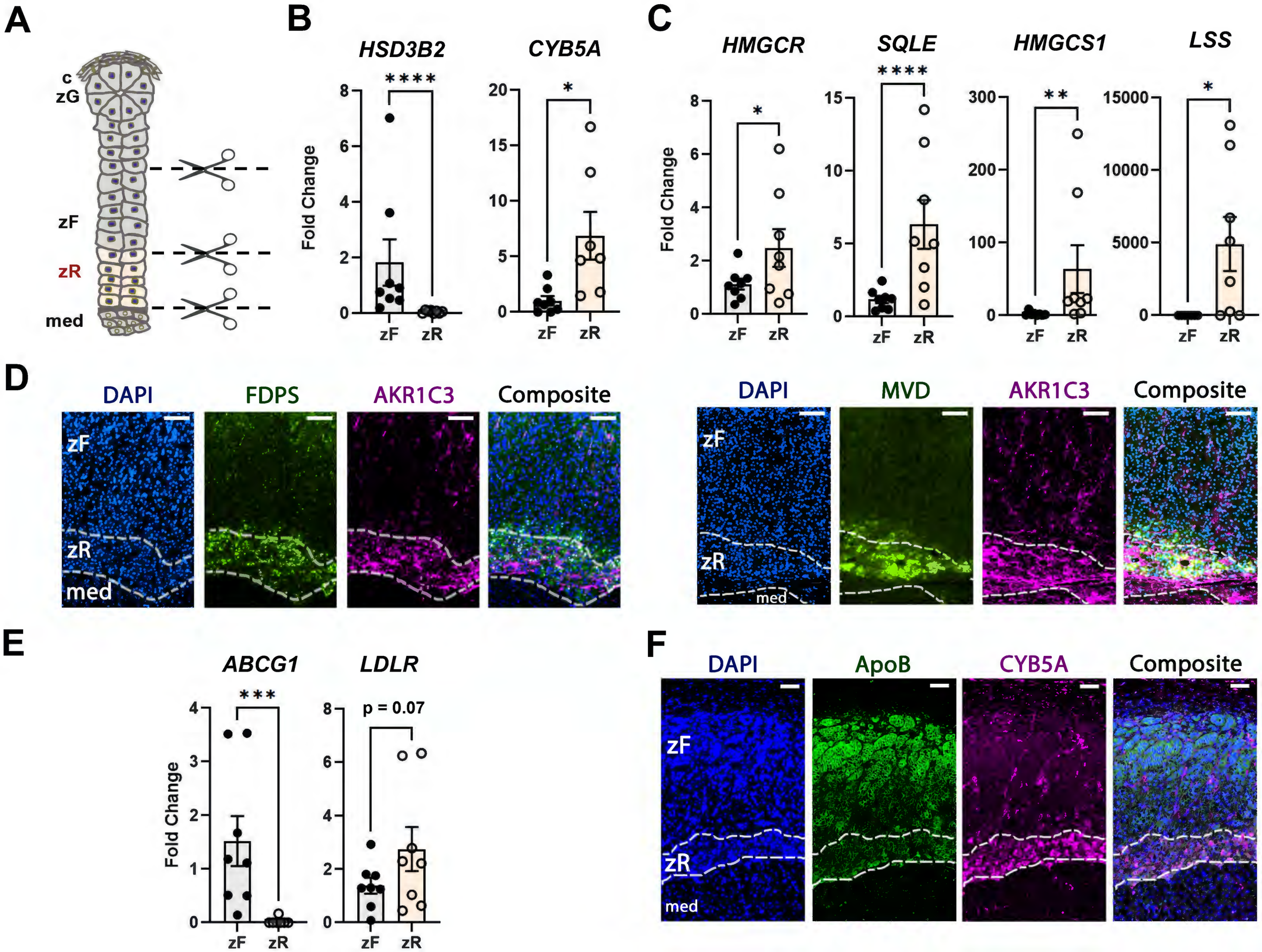
A
c
zG
zF
zR
med
B
HSD3B2
CYB5A
Fold Change
****
*
zF
zR
C
HMGCR
SQLE
HMGCS1
LSS
*
****
**
*
D
DAPI
FDPS
AKR1C3
Composite
MVD
zF
zR
med
E
ABCG1
LDLR
***
p = 0.07
F
DAPI
ApoB
CYB5A
Composite

Figure 2

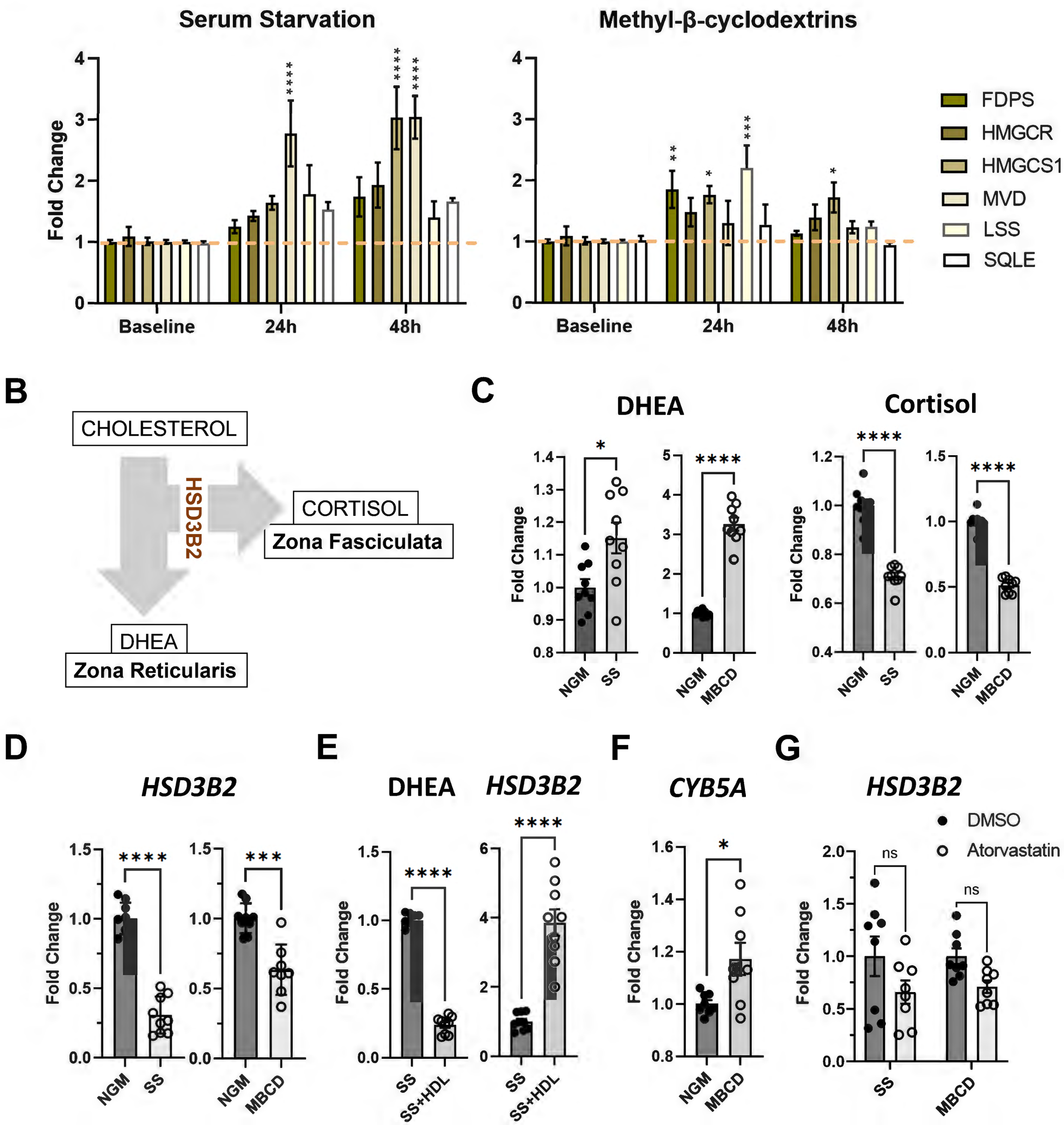
A
Serum Starvation
Methyl-β-cyclodextrins
Fold Change
Baseline
24h
48h
FDPS
HMGCR
HMGCS1
MVD
LSS
SQLE
B
CHOLESTEROL
HSD3B2
CORTISOL
Zona Fasciculata
DHEA
Zona Reticularis
C
DHEA
Cortisol
NGM
SS
MBCD
D
HSD3B2
E
DHEA
HSD3B2
SS
SS+HDL
F
CYB5A
G
HSD3B2
DMSO
Atorvastatin
ns

Figure 3

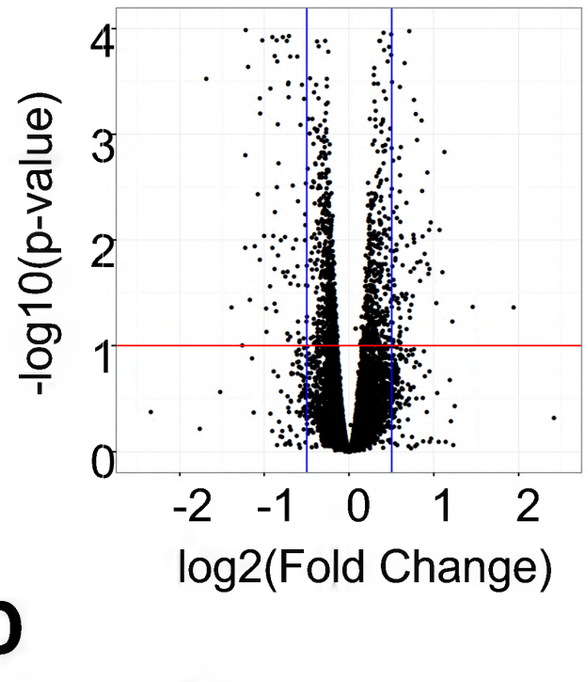
A
-log10(p-value)
log2(Fold Change)
4
3
2
1
0
-2
-1
0
1
2

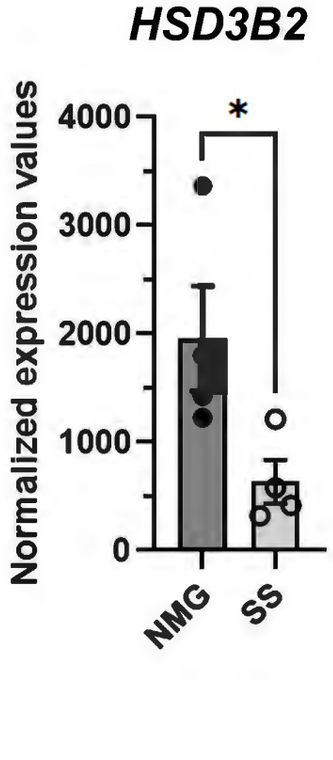
B
HSD3B2
Normalized expression values
4000
3000
2000
1000
0
*
NMG
SS

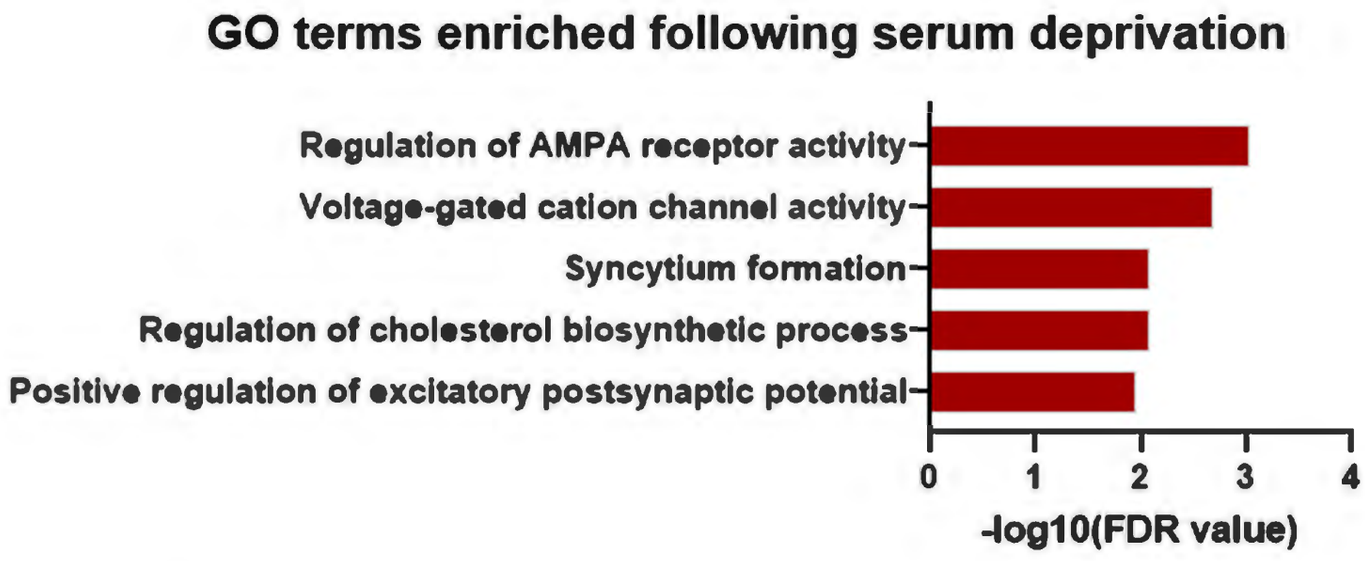
C
GO terms enriched following serum deprivation
Regulation of AMPA receptor activity
Voltage-gated cation channel activity
Syncytium formation
Regulation of cholesterol biosynthetic process
Positive regulation of excitatory postsynaptic potential
0
1
2
3
4
-log10(FDR value)

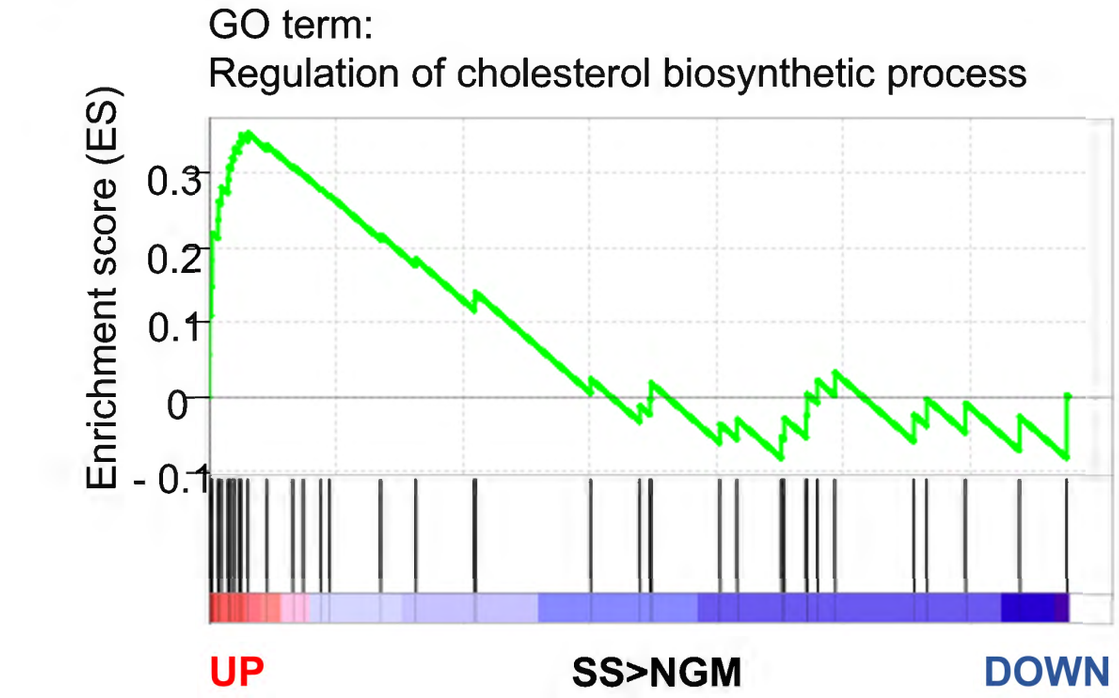
D
GO term:
Regulation of cholesterol biosynthetic process
Enrichment score (ES)
0.3
0.2
0.1
0
- 0.1
UP
SS>NGM
DOWN

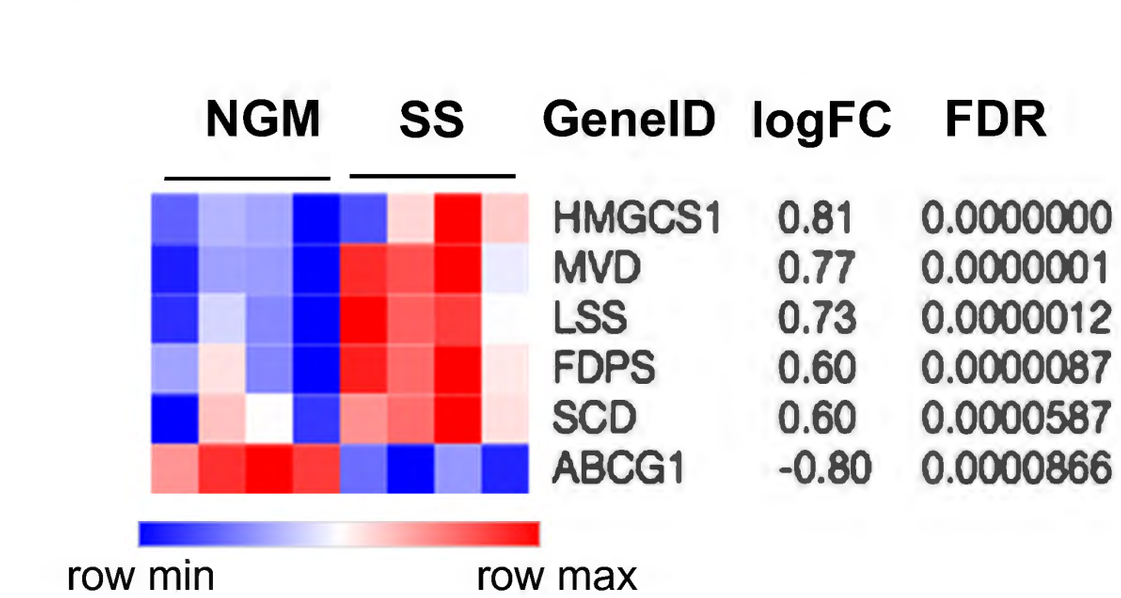
E
NGM
SS
GeneID
logFC
FDR
HMGCS1 0.81 0.0000000
MVD 0.77 0.0000001
LSS 0.73 0.0000012
FDPS 0.60 0.0000087
SCD 0.60 0.0000587
ABCG1 -0.80 0.0000866
row min
row max

Figure 4

A

Predicted transcription factors with differential activity following Serum Starvation

Transcription Factor(s)	Trend of activity in SS vs NGM	z-value TF	z-value *HSD3B2*
POU3F2	down	2.7	2.47
ELF2_GABPA_ELF5	down	3.34	1.71
ATF2_ATF1_ATF3	down	2.86	0.48
SIX5_SMARCC2_HCFC1	down	2.73	0.37
FOXM1_TBL1XR1	down	2.27	1